Chemical Geology 280 (2011) 323–335

Contents lists available at ScienceDirect

Chemical Geology

journal homepage: www.elsevier.com/locate/chemgeo

Germanium/silica ratios in diagenetic chert nodules from the Ediacaran Doushantuo Formation, South China

Bing Shen [a,*], Cin-Ty A. Lee [a], Shuhai Xiao [b]

[a] Department of Earth Science, Rice University, Houston, TX 77005, United States
[b] Department of Geosciences, Virginia Polytechnic Institute and State Univesity, Blacksburg, VA 24061, United States

ARTICLE INFO

Article history:
Received 8 April 2010
Received in revised form 9 November 2010
Accepted 10 November 2010
Available online 23 November 2010

Editor: U. Brand

Keywords:
Germanium
Silica
Chert nodule
Ediacaran
Doushantuo

ABSTRACT

Germanium/silica (Ge/Si) ratios of dolostone- and mudstone-hosted chert nodules from the Ediacaran (635–542 Ma) Doushantuo Formation in the Yangtze Gorges area, South China, are reported. These chert nodules typically have a calcite rim, a pyrite rim, and a silica core, the latter sometimes containing disseminated pyrite. The silica core was precipitated by early diagenetic replacement of carbonate and silty/muddy sediments. Two types of chert nodules are identified based on their mineralogy and geochemistry. Type-1 chert nodules are poor in disseminated pyrite in the silica core. They also have low Al, and show a strong positive correlation between Al contents and Ge/Si with a near-zero or negative intercept. In contrast, Type-2 chert nodules contain abundant disseminated pyrite in the silica core and show a weakly positive correlation between Ge/Si ratios and Al contents (with a large positive intercept on the Ge/Si axis). The Ge/Si of Doushantuo nodules are greater than those of Cretaceous deep-sea cherts, suggesting that the Ge/Si ratio of Ediacaran seawater/porewater was greater than the Cretaceous due to the more effective discrimination against Ge by inorganic opal precipitation relative to biogenic opal precipitation. The positive correlation between Ge/Si and Al can be interpreted using a mixing model with a pure chert (characterized by a low Ge/Si ratio) and an Al-rich endmember (characterized by a high Ge/Si ratio). The latter is most likely represented by a clay component, but the model-based estimate of the Ge/Si ratio inferred for the Al-rich (clay) endmember is much higher than that of Phanerozoic clay minerals. These high Ge/Si ratios for the clay endmember may be related to the generally high Ge/Si ratio of Ediacaran seawater, but could also be related to clay–organic matter interactions. Organic matter absorbed to clays could provide an additional source of Ge because certain organic molecules are known to have a high affinity for Ge due to their strong metal ion-chelating properties. The high Ge/Si ratio of the Al-rich endmember in Type-1 chert nodules suggests that Ge in porewaters from which these cherts precipitated may have been dominated by Ge–organic complexes. The low Ge/Si ratio inferred for the Al-rich endmember in Type-2 chert nodules is therefore taken to indicate that Ge was released from organic matter, perhaps due to anaerobic degradation of organic matter (accompanied by the formation of pyrite), and was redistributed between clay–organic endmembers and pure chert, resulting in a non-zero intercept in the Ge/Si vs. Al_2O_3 plots. These observations suggest that a strong terrestrial influence in a restricted sedimentary basin or a high content of dissolved organic carbon in Ediacaran seawater and porewater may have contributed to the dominance of Ge–organic complexes in the Doushantuo basin in the Yangtze Gorges area.

1. Introduction

The objective of this study is to understand Ge systematics in Precambrian aqueous environments. This is motivated by the fact that Ge, in particular the Ge/Si ratio, is an important biogeochemical index, which is sensitive to variations in weathering inputs, hydrothermal processes, and biological productivities (Froelich and Andreae, 1981; Froelich et al., 1985; Kurtz et al., 2002; Lugolobi et al., 2010; Wheat and McManus, 2008). Ge has a mixed distribution in the modern ocean, i.e. it is present in both inorganic and organic forms with substantially different behaviors (Bruland and Lohan, 2003). Inorganic Ge ($Ge(OH)_4$) shows a typical nutrient-type distribution due to utilization by diatoms in the surface ocean. However, because diatoms do not discriminate between Ge and Si, seawater has a homogeneous inorganic Ge/Si ratio of 0.72 (μmol/mol) that is determined by the influxes and sinks of both Ge and Si (Bareille et al., 1998; Froelich and Andreae, 1981; Froelich et al., 1985, 1989; Hammond et al., 2004; Mortlock and Froelich, 1987). River waters are the major source of seawater Si, accounting for ~80% of total Si influx to the ocean (DeMaster, 2002; Mortlock et al., 1993; Tréguer et al., 1995), whereas both hydrothermal and river waters are important contributors to Ge input into the ocean (Elderfield and Schultz, 1996; Mortlock et al., 1993). As for the sinks, biogenic opals account for nearly 100% of Si output,

* Corresponding author. MS126, 6100 Main St. Houston, TX 77005, United States. Tel.: +1 281 733 6317; fax: +1 713 348 5214.
E-mail address: bingshen66@gmail.com (B. Shen).

0009-2541/$ – see front matter © 2010 Elsevier B.V. All rights reserved.
doi:10.1016/j.chemgeo.2010.11.019

but only ~55% of Ge output; the remaining 45% of Ge output is attributed to non-opal minerals, such as Fe-rich clays in reduced sediments with high Fe^{2+} availability (Hammond et al., 2000; King et al., 2000; McManus et al., 2003). In contrast, methylgermanium, an organic complex with methyl groups that chelate with Ge, is the dominant organic Ge species in seawater, and shows a typical conservative distribution due to its extremely stable nature (Bruland and Lohan, 2003). The origin of methylgermanium in modern oceans is not completely understood, but is probably related to anthropogenic activities (Lewis et al., 1989). Due to the complex behavior of Ge and the decoupling of Ge and Si in seawater, variations in seawater Ge/Si may reflect changes in weathering inputs, hydrothermal activity, biological activity, and/or diagenetic processes in marine sediments.

Precambrian oceans, however, differ from modern oceans in the following aspects (Siever, 1992). In contrast to modern oxic deep oceans, Precambrian deep oceans were probably anoxic/euxinic throughout most of the Proterozoic (Canfield, 1998; Canfield et al., 2008), and are hypothesized to have been enriched in dissolved organic carbon (DOC) (Rothman et al., 2003). In addition, silica-secreting organisms, an important sink for both Ge and Si in modern oceans, were ecologically unimportant during the Proterozoic (Gehling and Rigby, 1996; Li et al., 1998; Siever, 1992; Steiner et al., 1993). Thus, it is reasonable to speculate that the Ge/Si systematics of Precambrian oceans would have behaved differently from their modern counterpart. However, there is no direct recorder of Proterozoic seawater Ge/Si because we know of no Proterozoic biogenic cherts. For this reason, we turn to early diagenetic chert nodules from the Ediacaran Doushantuo Formation in South China (635–551 Ma). These chert nodules were formed during early diagenesis (before compaction) through the replacement of carbonate sediments by silica precipitates (Xiao et al., 2010), and may thus record the Ge geochemistry of ancient porewaters, which in turn provide insight into seawater composition. We show here that the Ge/Si systematics of Doushantuo chert nodules is modulated by clay and organic matter, the latter suggesting that the Doushantuo porewater may be characterized by high DOC concentrations.

2. Geological setting

Chert nodules were collected from Member II of the Ediacaran (635–541 Ma) Doushantuo Formation at the Jiulongwan section (30°44.229′ N, 111°3.315′E) in the Yangtze Gorges area of the South China craton (McFadden et al., 2008, 2009). The Yangtze Gorges area is located in the northern part of the Yangtze Block, which lies to the northwest of the Cathaysia Block (Jiang et al., 2003; Li et al., 2007; Wang and Li, 2003) (Fig. 1). The Ediacaran strata in the Yangtze Gorges area are represented by the Sinian System. The upper boundary of the Sinian System is marked by the first appearance of the small shelly fossil *Anabarites trisulcatus–Protohertzina anabarica* assemblage, and the lower boundary by the base of the cap carbonate overlying the Nantuo diamictite (China Commission on Stratigraphy, 2001). The Nantuo diamictite is widely interpreted to be a glacial deposit equivalent to the terminal Cryogenian Elatina diamictite in Australia (Condon et al., 2005; Zhu et al., 2007). The *Anabarites trisulcatus–Protohertzina anabarica* assemblage is regarded as basal Cambrian (Qian, 1999).

The Ediacaran System in the Yangtze Gorges area consists of the Doushantuo and overlying Dengying formations (Zhao et al., 1988) (Fig. 2). The Doushantuo Formation, which has been the focus of extensive paleontological and geochemical investigations in the past decade (Xiao et al., 1998; McFadden et al., 2008, 2009; Zhu et al., 2008), is constrained to be between 635.2 ± 0.6 and 551.1 ± 0.7 Ma in the Yangtze Gorges area (Condon et al., 2005). At the Jiulongwan section, the Doushantuo Formation is approximately 155 m thick and divided into four lithological members (McFadden et al., 2009) (Fig. 2). Member I is represented by a cap dolostone containing sedimentary structures such as sheet cracks, tepee structures, macropeloids, and barite crystal fans

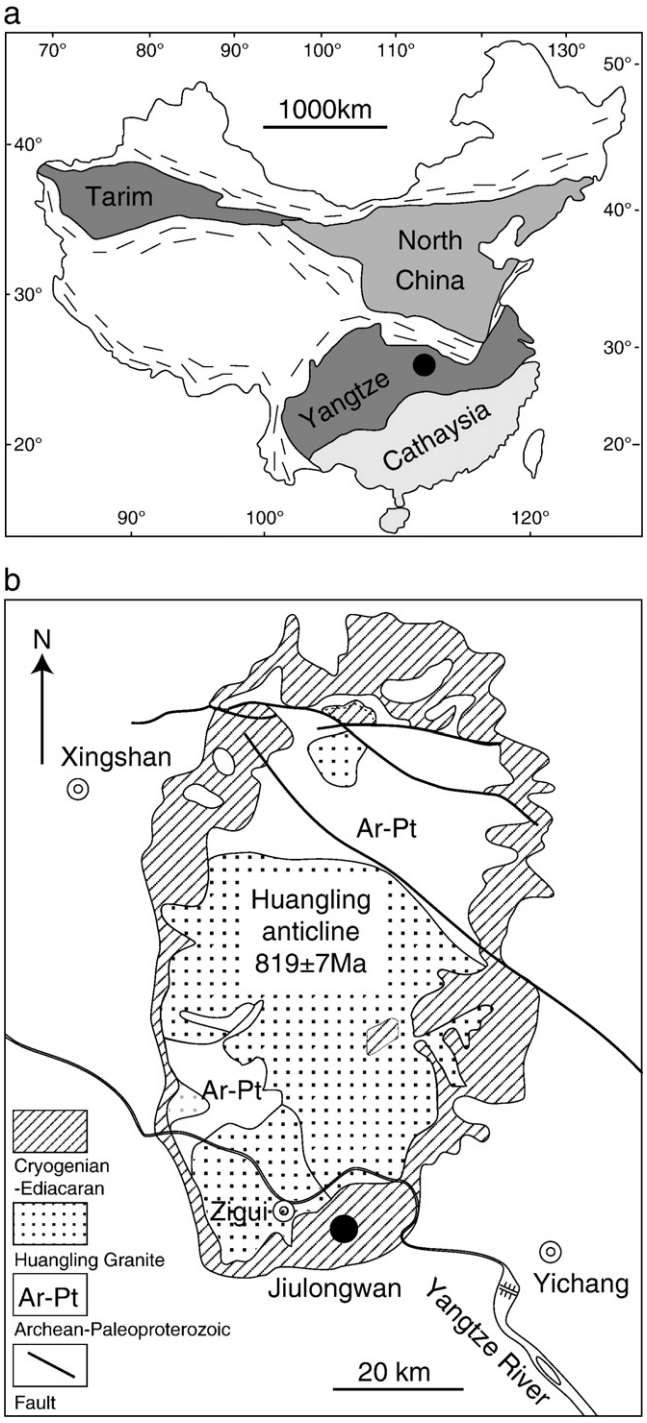

Fig. 1. (a) Map showing the geographic locality of the Yangtze Block and the Yangtze Gorges area (black dot). (b) Simplified geological map of the Yangtze Gorges area. The Jiulongwan section is marked by solid circle. From McFadden et al. (2008).

(Jiang et al., 2006). Member II is characterized by alternating black shale and shaley dolostone beds with abundant pea-sized chert nodules (Fig. 3a, b). Member III consists of massive and laminated dolostone overlain by interbedded limestone and dolomitic mudstone (ribbon rock). Member IV is a black organic-rich shale. The overlying Dengying Formation is represented by peritidal dolostone and organic-rich limestone deposited in a shallow water platform environment (Zhao et al., 1988), and is unconformably overlain by cherts, phosphorites, and dolostones of the Yanjiahe Formation, which yields basal Cambrian small shelly fossils and acritarchs (Chen, 1984; Dong et al., 2009).

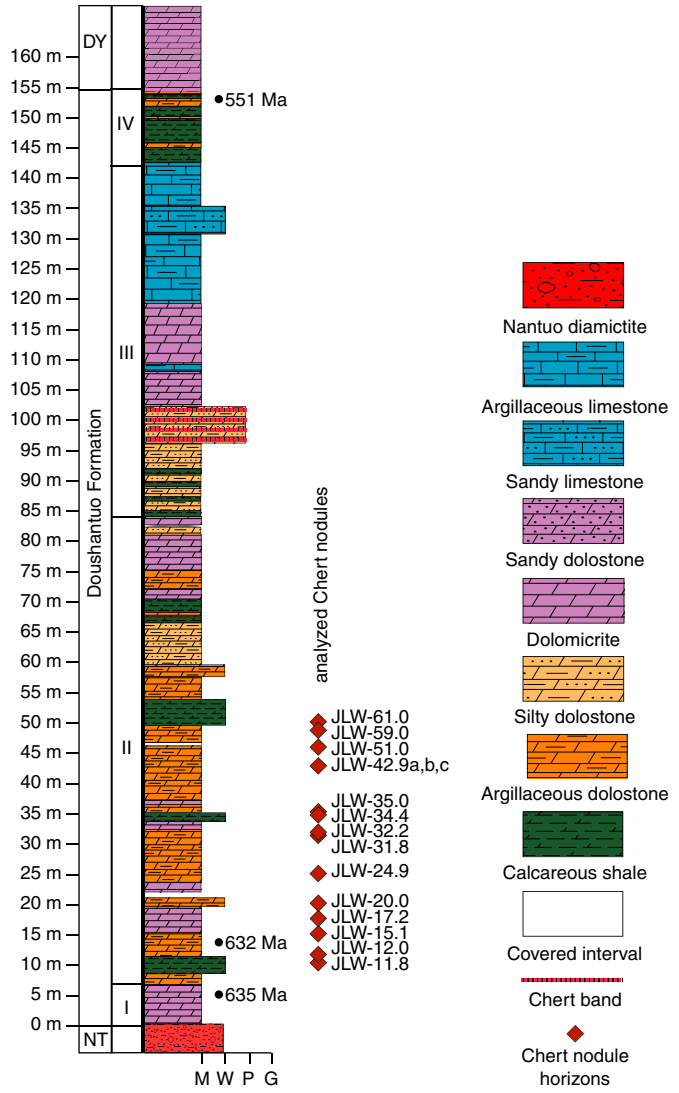

Fig. 2. Stratigraphic column of the Doushantuo Formation at the Jiulongwan section, Yangtze Gorges area, South China (from McFadden et al., 2008). Stratigraphic horizon of analyzed chert nodules are marked against the stratocolumn. DY: Dengying Formation; NT: Nantuo Formation.

There is no consensus on the depositional environment of the Doushantuo Formation in the Yangtze Gorges area. It has been traditionally interpreted as inner shelf marine deposits in the Yangtze Gorges area (Jiang et al., 2003; Wang and Li, 2003). This interpretation is supported by litho-, bio-, and chemostratigraphic relationships in South China (Vernhet et al., 2006; Zhou and Xiao, 2007; Zhou et al., 2007; Zhu et al., 2007). However, the lowermost 80 m of the Doushantuo Formation in the Yangtze Gorges area has recently been reinterpreted as being deposited in an alkaline lacustrine environment on the basis of high contents of saponite, a high-Mg low-K clay mineral normally precipitated under high pH (>9) conditions (Bristow et al., 2009). The balance of evidence from regional litho-, chemo-, and biostratigraphy indicates that the lower Doushantuo Formation in the Yangtze Gorges area was probably deposited in a restricted shelf basin with connections to the open ocean (Ader et al., 2009; Vernhet and Reijmer, 2010).

Chert nodules analyzed in this study were collected from a 50 m interval in Member II of the lower Doushantuo Formation (Fig. 2). This interval coincides with the first positive excursion in carbon isotopes in the Doushantuo Formation (EP 1) (McFadden et al., 2008, 2009; Zhou and Xiao, 2007; Zhu et al., 2007).

3. Doushantuo chert nodules

The Doushantuo chert nodules are hosted in four different lithologies: 1) organic-rich calcareous shale (clay>50%), 2) argillaceous dolostone, 3) silty dolostone, and 4) dolomicrite (Fig. 2). The chert nodules analyzed in this study are mainly hosted in dolostone and calcareous shale. Chert nodules vary from 1–3 cm in diameter (Fig. 3a, b) and contain abundant microfossils (McFadden et al., 2009). Individual chert nodules consist of microcrystalline quartz (Fig. 3c–f), but relicts of dolomicrites are abundant, suggesting that the chert nodules formed by diagenetic replacement of their host carbonate-bearing lithologies (Hesse, 1989; Maliva and Siever, 1989). Additional characteristics of the chert nodules are the presence of an early diagenetic pyrite rim and sometimes a late diagenetic calcite rim (Fig. 3b), which surround a silica core (Xiao et al., 2010). The weathering of the pyrite rim allows easy extraction of these chert nodules from the host rock. Disseminated pyrite is observed in the interior of some chert nodules (Fig. 3e, f). The disseminated pyrite includes randomly distributed subhedral crystals of a few tens to hundreds of microns in diameter (Fig. 3e, f). Based on the presence or absence of disseminated pyrite within the silica core, two types of Doushantuo chert nodules can be recognized: Type-1 (poor in disseminated pyrite, Fig. 3c, d) and Type-2 (rich in disseminated pyrite, Fig. 3e, f). In the context of their host rocks, Type-1 nodules are found in calcareous shale and argillaceous dolostone, whereas Type-2 nodules are found in all four lithologies.

Based on petrographic observations and geochemical data, it can be inferred that the Doushantuo chert nodules formed during early diagenesis, probably before compaction (Xiao et al., 2010). This inference is supported by the observation that (1) microbial laminations continue through the chert nodules and (2) microbial laminations in the matrix typically warp around chert nodules (Fig. 3a, b), suggesting that the nodules were lithified before compaction, perhaps near the water–sediment interface. Additional evidence for an early diagenetic origin comes from the presence of well preserved microfossils in the chert nodules (McFadden et al., 2009) and the highly positive $\delta^{34}S$ values of rim pyrite (Xiao et al., 2010). The early diagenetic origin of these chert nodules suggests that their chemistry reflects that of the pore-waters in uncompacted sediments.

4. Methods

Chert nodules were thin-sectioned and examined under a petrographic microscope. Major and trace element compositions were determined by laser ablation inductively coupled plasma mass spectrometry (LA-ICP-MS) at Rice University using a 213 nm laser (New-Wave) and a single-collector magnetic sector ICP-MS (ThermoFinnigan Element 2). Analyses were conducted in medium mass resolution ($m/\Delta m \sim 3000$). The following isotopes were measured: ^{7}Li, ^{23}Na, ^{25}Mg, ^{27}Al, ^{30}Si, ^{31}P, ^{39}K, ^{43}Ca, ^{45}Sc, ^{48}Ti, ^{51}V, ^{52}Cr, ^{55}Mn, ^{57}Fe, ^{59}Co, ^{60}Ni, ^{63}Cu, ^{66}Zn, ^{69}Ga, ^{74}Ge, ^{89}Y, and ^{91}Zr. At medium mass resolution, all significant isobaric interferences were resolved (e.g., $^{40}Ar^{16}O^{1}H^{+}$ was resolved from ^{57}Fe). Drift of the magnet (mass calibration) was corrected by centering on the $^{40}Ar^{40}Ar^{+}$ dimer during each run. Samples were ablated using a laser beam of 110 μm in diameter, at a 10 Hz pulse frequency, at a ~12 J/cm^2 energy density in line-scan mode, and at a velocity of 15 μm/s. A ~30 s gas background was taken while the laser was off, followed by ablation and acquisition of the signal. Background gas signals were subtracted from sample signals, and the resulting background-corrected signals were normalized to the ^{30}Si signal, which we used as an internal standard. External reference glass standards (United State Geological Survey basaltic glasses BHVO2g and BCR2g) were analyzed before the sequence of samples. In order to capture the compositional variations, four to six line scans were conducted for each nodule, and these line scans were oriented

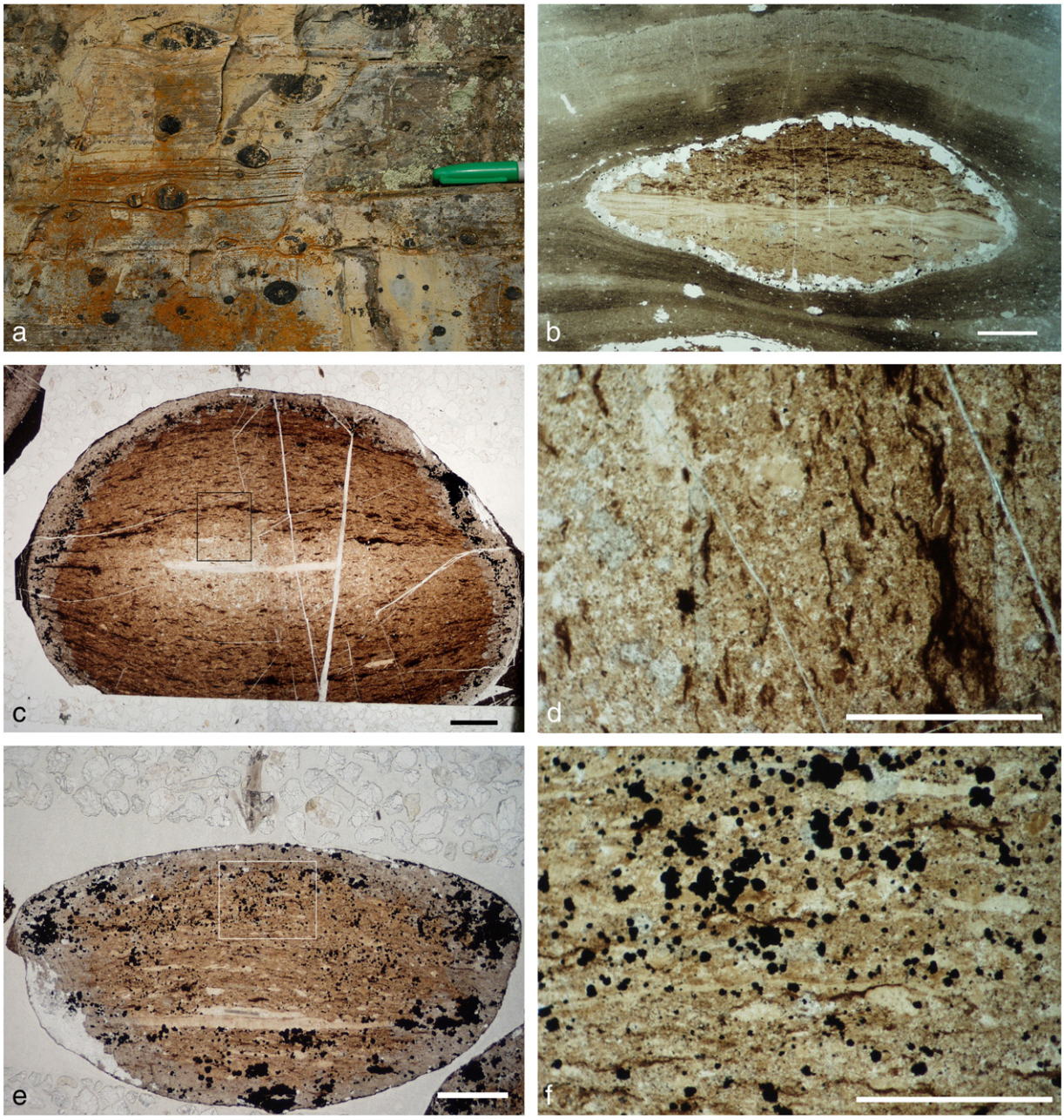

Fig. 3. Doushantuo chert nodules. (a) Field photographs of Doushantuo chert nodules. Pen cap (~5 cm) for scale. (b) Polished section of a Doushantuo chert nodule (sample number JLW-34.8). (c) Thin section photomicrography of a Type-1 chert nodule (sample number JLW-15.1). (d) Magnified view of rectangle area in (c). (e) Thin section photomicrography of a Type-2 chert nodule (sample number JLW-17.2). (f) Magnified view of rectangle area in (e), showing abundant disseminated pyrite. Scale bars are 0.5 mm in (c)–(f), and 1 mm in (b).

perpendicular to the radius and spaced at approximately equal distances from the center to the rim of the nodule.

Background-corrected signals were converted into elemental concentration ratios by calibration against BHVO2g and BCR2g external standards. For elemental ratios, such as Ge/Si, it is not necessary to precisely know the elemental concentration in the internal standard and samples. However, if all major and minor elements are measured, then elemental ratios can be used to calculate absolute concentrations. Absolute concentrations on a volatile-free basis (i.e., ignoring C, S, and H because these elements are not measured) were estimated by assuming all the measured major and minor elements as oxides (Na_2O, MgO, Al_2O_3, SiO_2, P_2O_5, K_2O, CaO, TiO, MnO, and FeO) and then summing up to 100% (Lee et al., 2008). There is a slight systematic bias in this approach because Ca and Mg could be in the form of carbonate and Fe could be in the form of Fe_2O_3 or FeS_2. However, the fact that the calculated SiO_2 contents are >95% (i.e., the chert nodules consist of nearly pure SiO_2) means that the volatile-free contents of other oxides are at worst biased by ~5%. These biases in absolute concentrations do not apply to elemental ratios, such as Ge/Si. Analytical uncertainties are calculated by multiple measurements of BHVO2g and BCR2g standards. The relative uncertainty of Ge/Si is better than 8% (1σ).

5. Results

Elemental compositions and Ge/Si ratios of the Doushantuo chert nodules are summarized in Table 1 and Figs. 4 and 5. Type-1 and Type-2 chert nodules share three geochemical characteristics: 1) both types of nodules have overlapping ranges of Ge/Si ratios, 2) Al content and Ge/Si ratio decrease from the rim to the core (Fig. 4), and 3) Na, K, Li,

Sc, Co, and Ga contents are positively correlated with Al content (Fig. 5). However, there are also some geochemical differences between these two types of chert nodules. Type-2 chert nodules have higher Al contents (0.62 ± 0.43 wt.%, 1σ) than Type-1 chert nodules (0.12 ± 0.05 wt.%) (Figs. 4 and 5). A striking feature is that, although the Ge/Si ratios between the two chert nodule types overlap (1.12 ± 0.54 μmol/mol in Type-1 and 1.25 ± 0.47 in Type-2), their Ge/Si–Al systematics differ. Type-1 chert nodules show positive correlations between Ge/Si and Al with regression lines having near-zero or negative intercepts and slopes ranging from 9.7 to 17.7 (Fig. 4). In contrast, Type-2 chert nodules show little to no co-variation between Ge/Si and Al. In those that do show a weak correlation, regression lines give large positive intercepts (~0.5 Ge/Si) and lower slopes between 0.05 and 1.36 (Fig. 4).

6. Discussion

6.1. Ge/Si systematics of chert nodules

Although a wide range of Ge/Si ratios has been observed in individual chert nodules, the two types of nodules have overlapping ranges of Ge/Si ratios. Most samples have their maximum Ge/Si ratio exceeding 1, significantly greater than that of bulk Cretaceous deep-sea chert (Rouxel et al., 2006). This disparity suggests that Ge/Si ratios of the Doushantuo seawater/porewater might have been higher than that of Cretaceous seawater. Considering that silica-secreting organisms (e.g. diatoms and radiolarians) were not ecologically important in the Ediacaran ocean, inorganic opal precipitation may have been the predominant Si sink in Ediacaran oceans (Siever, 1992). Unlike diatoms that do not appear to discriminate against Ge (Bareille et al., 1998), inorganic SiO_2 formation can discriminate against Ge more effectively. The estimated fractionation factor of Ge/Si [defined as $\alpha = (Ge/Si)_{quartz}/(Ge/Si)_{fluid}$] of hydrothermal cherts precipitated from the Himalaya hydrothermal hot-springs ranges from 0.023 to 0.0054, suggesting significant discrimination against Ge during inorganic quartz precipitates (Evans and Derry, 2002). Therefore, the dominance of inorganic opal precipitation in Ediacaran oceans would drive the seawater Ge/Si to be substantially higher than post-diatom oceans.

However, the positive correlation between Ge/Si and Al content (evaluated in Al_2O_3 wt.%) in all Type-1 and some Type-2 chert nodules suggests that an Al-rich component may have played a role in enhancing the Ge/Si ratios. This correlation can be explained by the binary mixing between a pure chert endmember (with a low Ge/Si ratio and zero Al content) and an Al-rich endmember characterized by a high Ge/Si ratio. The low Ge/Si ratio of the pure chert member, despite possibly high Ge/Si ratios in Ediacaran seawater, might be related to effective discrimination against Ge by inorganic opal precipitation (Evans and Derry, 2002). As for the Al-rich endmember, positive correlations between Na, K, Li, and Ga with Al contents strongly suggest that the Al-rich endmember is controlled by clay minerals (Fig. 5) because these elements are either major or trace elements in clay minerals and absent in chert. Clay minerals have been reported to have high Ge/Si ratios [typically >2; (Bernstein, 1985; Rouxel et al., 2006)], and could explain the positive correlations between Ge/Si and Al in the chert nodules. The rim-to-core decrease in Al content (Fig. 4) could be due to the centrifugal displacement of clays during the precipitation of silica core (Xiao et al., 2010). The binary clay–chert mixing can be described using a simple mass balance equation:

$$(Ge/Si)_{nodule} = \frac{f \times (Ge/Si)_{alum} \times Si_{alum} + (1-f) \times (Ge/Si)_{SiO2} \times Si_{SiO2}}{f \times Si_{alum} + (1-f) \times Si_{SiO2}} \quad (1)$$

where $(Ge/Si)_{nodule}$ is the Ge/Si of the chert nodule, f is the mass fraction of the Al-rich endmember, $(Ge/Si)_{alum}$ and $(Ge/Si)_{SiO2}$ are the Ge/Si ratios of the Al-rich and pure chert endmembers, and Si_{alum} and Si_{SiO2} are the Si contents (SiO_2 wt.%) of the Al-rich and pure chert endmembers (chert Si content is assumed to be equivalent to 100 wt. % SiO_2). Because the pure chert endmember is assumed to have zero Al content, the Al content of the chert nodule is given by:

$$Al_{nodule} = f \times Al_{alum} \quad (2)$$

where Al_{nodule} and Al_{alum} are the Al content (Al_2O_3 wt.%) of the chert nodule and Al-rich endmember. Thus, in a $(Ge/Si)_{nodule}$–Al_{nodule} plot, the y-intercept of a binary mixing line, where Al_{nodule} and f equal zero, is equal to the Ge/Si ratio of the pure chert endmember, i.e., $(Ge/Si)_{SiO2}$.

Taking $(Ge/Si)_{SiO2}$ as equivalent to the y-intercept in Fig. 4b (using 0 for Type-1 and ~0.5 for Type-2 nodules), Eq. (1) can be used to construct binary mixing lines for any Ge/Si ratio of the Al-rich endmember (i.e., $(Ge/Si)_{alum}$). To estimate the range of $(Ge/Si)_{alum}$, we plot the calculated mixing lines and the measured Doushantuo data into the same Ge/Si–Al space (Fig. 6). This method is better than direct extrapolation from plots in Fig. 4b, because large extrapolation could generate large errors and not all samples show correlation. The most likely clays in these chert nodules and in the host sediments are illites and smectites. Illites have Al_2O_3/SiO_2 mass ratios of 0.74–0.84. Typical marine smectites have Al_2O_3/SiO_2 mass ratios of ~0.2–0.3 (Awwiller, 1993). Saponitic smectites, which occur in Member II black shales of the Doushantuo formation (Bristow et al., 2009), have Al_2O_3/SiO_2 mass ratios ~0.1. Assuming Al_2O_3/SiO_2 of the clay endmember to be 0.25 (e.g., representative of smectite), we find that $(Ge/Si)_{alum}$ of most Type-1 chert nodules lies between 100 and 400 (Fig. 6a). In Type-2 chert nodules, $(Ge/Si)_{alum}$ vary between 10 and 200, with most between 20 and 100 (Fig. 6b). If we had used a higher Al/Si ratio characteristic of illite, the estimated Ge/Si ratios of the Al-rich endmember would be even higher, so these calculations should be taken as minimum estimates based on the two-member mixing model. Even so, these Ge/Si ratios are still 1–2 orders of magnitude higher than Ge/Si of modern marine clay minerals (2–4) (Rouxel et al., 2006).

To place the Doushantuo chert nodules in broader context, we apply the same calculations to Cretaceous deep-sea cherts. Unlike the Doushantuo chert nodules, which have a diagenetic origin, the Cretaceous cherts are siliceous sediments formed by direct deposition of diatom frustules or aqueous precipitation from Si-laden bottom waters, where dissolved Si ultimately also originate from dissolution of diatoms. Interestingly, Cretaceous deep-sea cherts also show positive correlation between Al and K contents (Rouxel et al., 2006), suggesting possible incorporation of clay minerals. If we put the Cretaceous deep-sea chert data in the same mixing model with the y-intercept at ~0.4, we find $(Ge/Si)_{alum}$ for Cretaceous deep-sea cherts to be 1–5, which is consistent with the Ge/Si of marine clay minerals. In comparison, the inferred $(Ge/Si)_{alum}$ values for the Doushantuo chert nodules are anomalously high relative to Phanerozoic clays.

6.2. Origin of high Ge/Si in clay-rich component

One possible interpretation for the anomalously high $(Ge/Si)_{alum}$ values is that this Al-rich endmember represents authigenic clays that were precipitated from porewater with extremely high Ge/Si. Ge/Si ratios of porewaters in modern marine environments are typically around 0.1–1 (Hammond et al., 2000; McManus et al., 2003), with rare exceptions (King et al., 2000; Wheat and McManus, 2008) where they can approach the $(Ge/Si)_{alum}$ inferred from the Doushantuo chert nodules. In Ediacaran marine environments, however, porewaters and hence authigenic clays could have had much greater Ge/Si ratios (see above), leading to greater $(Ge/Si)_{alum}$ ratios. With regard to the two types of Doushantuo nodules, because $(Ge/Si)_{alum}$ is higher for Type-1 than Type-2 nodules, authigenic clay component in Type-1 chert nodules must have precipitated from porewaters with greater Ge/Si ratios. If the pure-chert endmember and the clay endmember were

Table 1
Elemental compositions and Ge/Si ratios of Doushantuo chert nodules. SN: sample number; #: sequence of measurement (1: outer rim; 8: inner core); type I chert nodules are denoted in italic with [a].

SN	#	Ge/Si	Na_2O	MgO	Al_2O_3	SiO_2	K_2O	CaO	FeO	Ge	Li	P	Sc	Ti	Mn	V	Cr	Co	Ni	Cu	Zn	Ga	Y	Zr
		μmol/mol	%	%	%	%	%	%	%	ppm	ppm	ppm	ppm	ppm	ppm	ppm	ppm	ppm	ppm	ppm	ppm	ppm	ppm	ppm
JLW-11.8[a]	3	1.90	0.0922	0.289	0.150	98.6	0.0405	0.699	0.169	2.36	5.53	71.0	0.198	295	66.5	8.08	4.90	0.356	4.31	9.46	9.61	1.01	0.777	6.82
	4	1.75	0.0804	0.714	0.133	97.9	0.0347	0.964	0.164	2.15	5.12	58.0	0.189	250	61.3	6.46	3.46	0.557	5.47	9.97	6.12	0.906	0.943	5.52
	5	1.23	0.0455	0.450	0.0826	99.0	0.0252	0.308	0.130	1.53	2.86	40.0	0.0774	84.0	33.6	2.34	1.74	0.307	3.53	4.73	8.95	0.727	0.404	3.16
	6	1.56	0.0666	1.07	0.112	97.8	0.0303	0.801	0.160	1.92	3.36	67.6	0.155	134	56.7	3.55	2.08	0.367	4.08	10.1	8.56	0.798	0.727	4.69
	7	1.08	0.0529	0.265	0.106	98.8	0.0313	0.402	0.307	1.34	3.26	126	0.106	78.0	34.2	1.86	1.79	0.722	7.72	9.42	7.05	0.615	0.909	2.55
	8	1.54	0.0643	0.466	0.108	98.8	0.0269	0.448	0.0714	1.91	3.47	40.2	0.131	134	44.2	3.08	3.30	0.201	2.44	5.66	4.81	0.732	0.386	2.72
JLW-12[a]	2	1.29	0.0604	0.661	0.118	98.1	0.0323	0.847	0.149	1.53	3.46	168	0.135	56.4	56.0	1.49	2.55	0.444	3.60	8.42	8.77	1.20	1.04	5.46
	3	1.05	0.0682	0.225	0.095	99.0	0.0357	0.402	0.139	1.26	3.21	429	0.0915	92.6	35.3	2.08	2.88	0.506	4.11	18.9	5.23	1.39	1.43	5.84
	4	0.703	0.0944	0.162	0.0828	98.9	0.0634	0.611	0.109	0.841	3.58	73.2	0.120	90.6	29.6	2.09	1.93	0.279	3.19	6.24	5.24	1.30	0.576	3.56
	5	0.76	0.0676	0.339	0.0735	98.9	0.0358	0.485	0.103	0.912	2.83	39.6	0.101	66.0	21.6	1.60	1.97	0.219	1.85	4.47	13.92	1.35	0.359	4.77
	6	0.606	0.0545	0.0217	0.0944	99.1	0.0311	0.554	0.189	0.726	2.33	36.5	0.0914	38.1	29.7	0.669	1.50	0.360	3.45	5.44	5.67	1.40	0.191	4.12
JLW-15.1[a]	2	1.49	0.0766	0.350	0.200	93.7	0.0290	5.38	0.224	1.69	24.6	939	0.183	80.5	175	2.46	4.73	0.497	3.27	5.11	2.97	1.21	2.09	3.61
	3	1.26	0.0604	0.302	0.162	97.0	0.0258	2.26	0.198	1.48	7.03	1790	0.205	61.0	159	1.48	2.34	0.362	2.81	4.00	5.38	1.39	1.55	4.07
	4	0.657	0.0484	0.0444	0.125	99.1	0.0258	0.490	0.174	0.788	3.84	967	0.103	102	19.5	2.92	1.93	0.460	1.93	3.95	2.43	1.43	0.594	3.22
	5	0.349	0.0254	0.0395	0.0649	99.7	0.0250	0.095	0.0557	0.421	1.45	15.0	0.0640	59.4	7.25	0.376	0.794	0.208	1.76	3.07	4.52	0.495	0.0919	2.57
	6	0.219	0.0224	0.105	0.0831	93.8	0.0128	5.78	0.137	0.248	10.5	168	0.0668	20.1	77.6	0.360	1.03	0.173	1.50	3.45	7.24	0.659	2.07	1.60
JLW-17.2	1	1.01	0.207	1.06	0.689	85.0	0.104	0.362	12.6	1.03	61.1	59.9	0.311	177	24.0	2.61	3.20	0.613	2.95	10.9	5.92	2.58	0.652	5.34
	2	1.07	0.151	0.522	0.460	88.7	0.0571	0.346	9.76	1.14	34.9	25.1	0.232	145	37.2	3.05	3.75	0.626	2.90	5.64	12.9	2.56	0.640	9.75
	3	1.08	0.127	0.397	0.374	94.5	0.0751	0.424	4.14	1.23	45.8	29.8	0.375	427	27.5	5.35	3.52	0.877	2.54	3.88	3.31	2.45	1.03	20.0
	4	0.912	0.146	0.672	0.405	97.7	0.0642	0.364	0.627	1.08	42.6	23.8	0.255	224	55.5	3.70	3.32	0.837	2.62	3.46	3.94	2.52	0.310	10.7
	5	0.872	0.0322	0.00429	0.0620	99.8	0.0140	0.05	0.0282	1.05	3.59	5.68	0.0703	56.1	4.09	0.257	1.18	0.04	0.573	0.86	1.80	2.27	0.0267	9.02
	6	1.22	0.143	1.87	0.760	95.0	0.0806	0.340	1.75	1.40	62.6	105	0.375	376	36.4	5.55	4.53	1.17	3.09	5.34	10.5	3.76	0.451	10.8
JLW-20[a]	1	2.32	0.103	0.144	0.147	99.0	0.0529	0.382	0.132	2.78	7.05	83.9	0.107	76.6	25.1	0.806	3.18	0.368	3.86	8.72	2.96	1.50	0.486	4.29
	2	1.59	0.0839	0.227	0.130	99.0	0.0437	0.289	0.184	1.91	5.95	56.9	0.0969	63.3	21.0	1.64	3.43	0.389	3.49	5.37	2.68	1.52	0.137	1.64
	3	1.46	0.0601	0.204	0.130	99.1	0.0336	0.186	0.277	1.75	2.29	20.6	0.0889	69.7	19.8	2.06	2.57	0.529	4.49	9.72	5.45	0.984	0.105	2.13
	4	0.83	0.0487	0.124	0.0870	98.6	0.0226	0.934	0.144	0.986	1.77	174	0.0967	61.8	27.3	1.75	2.48	0.348	3.07	6.26	3.26	0.787	0.339	1.29
	5	0.49	0.0316	0.0943	0.0480	99.0	0.0151	0.347	0.474	0.587	1.11	75.7	0.0718	75.9	16.1	1.27	2.16	0.276	2.45	7.44	3.30	0.659	0.174	1.35
	6	0.0408	0.0174	0.00209	0.0426	99.9	0.0076	0.00919	0.0598	0.0493	0.0876	3.39	0.0310	1.78	6.96	0.08	0.975	0.0367	0.920	1.54	1.28	0.754	0.000	0.767
JLW-24.9	1	1.93	0.443	3.05	1.27	90.2	0.251	3.71	1.07	2.10	261	38.0	0.312	348	139	4.90	8.59	2.82	14.3	41.3	9.54	2.82	0.581	15.6
	2	1.78	0.341	1.57	0.947	95.9	0.199	0.349	0.647	2.06	132	33.3	0.206	297	73.8	5.26	5.64	2.21	14.4	45.0	9.60	2.59	0.576	7.32
	4	1.98	0.251	0.585	0.342	97.2	0.134	1.09	0.381	2.33	24.2	50.9	0.541	404	45.2	8.96	7.64	1.49	6.81	19.7	20.2	2.07	1.09	11.7
	5	2.27	0.293	0.530	0.369	97.9	0.151	0.499	0.248	2.69	28.0	51.1	0.560	343	39.8	10.8	6.17	1.36	5.34	17.8	13.8	1.12	0.896	9.70
	6	2.54	0.191	0.483	0.217	98.3	0.0837	0.549	0.221	3.02	12.3	41.5	0.495	411	39.0	7.79	5.02	1.09	4.05	7.93	8.73	0.720	0.42	4.10
JLW-31.8	1	2.22	0.421	3.41	1.61	92.8	0.307	0.577	0.856	2.50	196	25.6	0.306	187	42.0	6.85	8.18	2.20	17.2	86.9	11.1	4.46	0.71	17.7
	2	1.73	0.324	1.53	0.868	95.9	0.232	0.513	0.586	2.01	81.9	69.3	0.195	141	48.4	4.36	4.44	1.15	8.17	37.0	192	2.86	0.73	7.27
	3	1.26	0.243	0.879	0.535	97.0	0.158	0.422	0.773	1.48	49.6	69.3	0.214	196	40.4	5.47	4.35	2.09	9.38	16.1	11.8	2.60	0.810	7.13
	4	1.39	0.252	0.709	0.584	96.2	0.212	0.257	1.78	1.61	40.2	58.0	0.194	357	125	6.93	4.09	4.48	12.0	28.3	301	2.66	0.74	6.79
	5	1.08	0.196	0.408	0.386	98.3	0.172	0.210	0.346	1.28	35.0	41.2	0.219	1040	16.8	5.36	4.30	1.14	6.12	14.4	10.4	1.24	1.42	11.1
	6	2.18	0.171	0.341	0.345	98.8	0.0997	0.127	0.0927	2.61	28.9	14.8	0.091	108	8.93	2.07	2.79	0.398	3.96	12.6	6.07	1.48	0.214	9.12
JLW-32.2	1	1.48	0.114	0.470	0.320	98.4	0.0692	0.216	0.455	1.76	20.6	87.2	0.117	133	21.8	2.92	3.10	1.06	5.22	14.4	9.82	1.25	0.719	6.73
	2	1.27	0.204	1.27	0.776	91.3	0.140	5.73	0.527	1.40	49.3	184	0.286	468	70.1	6.74	7.02	1.86	8.54	20.9	6.21	1.48	6.34	10.3
	3	1.16	0.232	0.700	0.479	97.9	0.191	0.235	0.224	1.37	33.8	37.5	0.180	246	26.3	4.47	3.64	0.855	6.90	10.8	5.09	1.51	0.931	10.4

	4	1.13	0.235	0.150	0.448	98.0	0.226	0.0922	0.844	1.34	42.8	37.9	0.228	282	21.3	4.68	4.28	0.622	3.96	10.9	4.15	1.51	0.759	8.81
	5	0.764	0.221	0.0514	0.228	98.8	0.0807	0.0824	0.492	0.914	14.6	60.3	0.161	170	20.0	3.47	3.25	1.05	5.99	14.6	7.29	1.32	0.567	9.07
	6	0.800	0.197	0.0277	0.160	99.2	0.0574	0.0576	0.260	0.961	9.86	18.4	0.108	94.8	11.5	1.89	2.10	0.454	2.21	7.12	4.32	1.54	0.198	10.4
JLW-34.4	3	1.09	0.171	0.536	0.506	97.7	0.252	0.106	0.753	1.29	35.2	70.6	0.329	373	14.0	7.49	3.24	1.39	4.95	20.4	237	2.56	3.08	24.7
	4	1.05	0.132	0.233	0.329	82.5	0.174	0.425	16.21	1.05	16.6	76.6	0.202	103	10.4	2.27	2.47	1.31	3.52	31.2	15.2	1.92	0.866	15.2
	5	1.17	0.176	0.949	0.663	96.1	0.290	0.128	1.68	1.36	47.8	42.1	0.295	222	16.4	6.02	4.35	2.06	7.55	16.4	16.8	2.99	0.863	18.7
	6	0.984	0.187	1.06	0.676	96.3	0.232	0.539	1.00	1.15	48.0	68.5	0.276	248	17.5	5.58	3.33	1.51	4.89	13.7	7.92	2.47	2.16	16.3
JLW-35	1	1.62	0.209	2.66	0.778	94.4	0.120	1.41	0.456	1.85	75.2	133	0.250	129	56.2	5.06	6.02	1.11	6.52	18.5	5.83	3.68	1.22	8.79
	2	1.72	0.210	0.831	0.303	96.3	0.101	1.31	0.935	2.01	13.9	297	0.188	356	53.9	6.83	8.77	1.07	6.65	14.2	4.74	2.13	2.36	7.01
	3	1.85	0.124	0.172	0.145	98.9	0.0409	0.270	0.308	2.22	8.09	50.8	0.186	136	24.8	2.13	4.33	0.597	3.09	7.31	5.30	1.22	0.253	8.72
	4	0.666	0.0515	0.0303	0.125	97.6	0.0294	1.62	0.581	0.786	3.36	675	0.236	127	29.1	2.09	4.08	0.857	4.78	11.3	6.01	1.43	2.05	9.24
	5	0.303	0.0382	0.0511	0.100	94.9	0.0177	4.74	0.112	0.348	0.605	34.7	0.106	34.6	35.3	1.30	1.79	0.076	1.05	2.25	1.86	1.32	0.845	11.6
JLW-42.9A	1	1.98	0.391	1.37	1.28	95.5	0.571	0.428	0.499	2.29	87.7	101	0.457	629	40.3	6.84	8.08	1.85	9.94	45.7	6.29	3.87	1.49	8.71
	2	1.46	0.233	1.46	0.868	94.8	0.376	1.12	1.17	1.67	47.4	107	0.554	2150	51.3	18.4	7.58	2.29	8.48	21.4	24.9	3.10	2.81	12.6
	3	1.12	0.180	0.370	0.528	97.3	0.2776	0.147	1.20	1.32	28.3	44.1	0.267	206	23.0	4.18	3.99	1.53	4.71	14.7	10.3	1.85	1.00	8.16
	4	0.837	0.194	0.174	0.479	93.0	0.424	0.0847	5.62	0.942	26.0	30.2	0.175	314	22.2	3.22	2.87	1.99	6.69	23.5	10.6	1.01	0.744	6.49
	5	0.775	0.0450	0.0124	0.0901	99.7	0.0256	0.0413	0.08	0.935	2.21	84.3	0.100	65.2	7.19	1.40	1.24	0.119	1.39	1.94	2.05	0.837	0.561	4.70
	6	0.669	0.0794	0.00490	0.163	99.5	0.0297	0.0405	0.184	0.806	3.08	29.0	0.180	57.5	6.79	0.804	0.951	0.322	1.86	3.94	2.30	1.12	0.144	4.73
JLW-42.9B	1	1.02	0.115	1.58	0.893	95.4	0.503	0.604	0.854	1.17	62.6	213	0.474	609	63.8	9.48	6.40	2.07	7.18	19.8	12.9	3.09	1.16	14.3
	2	0.980	0.099	0.369	0.661	93.2	0.273	0.796	4.58	1.11	38.2	165	0.428	197	61.6	6.18	6.10	1.39	7.83	27.3	48.2	2.22	1.09	12.8
	3	0.878	0.101	0.410	0.587	93.9	0.414	0.242	4.35	1.00	43.1	337	0.548	343	45.3	7.69	6.48	1.86	9.04	28.6	58.2	2.97	2.51	12.0
	4	0.805	0.124	0.468	0.629	94.7	0.530	0.379	3.15	0.923	49.1	418	0.510	455	59.5	8.17	7.39	2.74	10.7	38.1	83.7	2.90	1.53	14.5
	5	1.05	0.103	0.575	0.731	92.0	0.358	0.436	5.75	1.17	48.9	1210	0.427	384	76.5	6.37	9.67	3.66	14.6	51.8	33.4	2.91	3.38	16.7
	6	1.10	0.122	1.06	1.02	92.7	0.415	1.78	2.90	1.23	69.2	253	0.387	331	65.1	8.05	9.63	2.76	13.1	31.8	34.4	3.09	1.74	10.7
JLW-42.9C	1	1.23	0.296	1.51	1.09	95.0	0.505	0.522	1.02	1.42	66.2	208	0.563	745	79.6	12.7	9.30	4.78	16.8	30.0	247	3.83	1.54	10.2
	2	1.29	0.272	0.582	0.667	96.9	0.366	0.167	1.05	1.52	57.5	125	0.293	364	72.5	6.56	6.56	3.30	13.2	29.3	665	3.95	1.27	10.1
	3	1.31	0.269	0.329	0.623	95.7	0.284	0.189	2.56	1.52	44.9	85.8	0.296	308	71.4	5.88	5.61	3.36	13.1	33.1	62.1	2.24	1.03	10.4
	4	0.873	0.318	0.598	0.780	95.4	0.224	0.510	2.21	1.01	61.7	1180	0.340	439	48.0	8.45	27.3	3.18	9.84	25.0	20.8	3.03	3.48	8.13
	5	1.00	0.166	0.0336	0.206	98.3	0.0587	0.121	1.14	1.19	16.5	163	0.255	110	31.8	1.66	2.56	1.21	4.86	10.3	11.2	1.68	0.658	4.76
	6	0.985	0.125	0.0183	0.166	99.4	0.0420	0.0788	0.209	1.18	6.19	172	0.194	205	8.64	2.92	2.64	0.284	1.67	4.43	8.25	1.61	0.887	6.84
JLW-51	2	1.62	0.328	1.16	0.708	95.5	0.318	1.57	0.387	1.87	65.5	1010	0.336	262	23.0	4.57	8.71	0.993	5.53	16.8	69.6	2.93	3.82	10.2
	3	1.34	0.207	0.540	0.435	97.1	0.227	0.787	0.729	1.57	38.2	218	0.240	211	27.4	3.80	9.12	1.33	5.87	19.9	40.3	2.51	1.72	6.75
	4	1.20	0.251	0.652	0.640	97.1	0.203	0.245	0.880	1.41	43.3	139	0.221	314	28.6	5.30	7.64	1.58	6.39	14.2	23.6	2.28	1.04	7.27
	5	1.06	0.233	0.487	0.523	97.5	0.208	0.195	0.836	1.25	38.9	93.6	0.219	230	26.5	4.89	7.75	1.18	5.44	13.8	92.9	1.55	1.24	9.81
	6	0.924	0.188	0.462	0.380	95.9	0.148	0.458	2.51	1.07	23.7	746	0.147	124	24.0	2.46	3.95	0.992	4.35	14.7	14.9	1.44	1.87	6.19
JLW-59[a]	1	1.53	0.159	0.0350	0.201	99.2	0.0667	0.0711	0.301	1.83	11.2	18.4	0.110	78.9	32.6	1.15	5.31	0.622	5.25	12.2	1.75	2.72	0.60	9.58
	2	1.59	0.142	0.0258	0.194	98.5	0.0564	0.940	0.167	1.90	7.02	57.4	0.137	53.5	18.2	0.789	3.53	0.282	3.80	5.05	3.22	2.09	1.05	13.4
	4	0.847	0.0860	0.0118	0.165	99.5	0.0366	0.0400	0.178	1.02	2.65	50.9	0.079	57.1	14.1	0.637	2.42	0.280	2.18	4.35	1.86	1.74	0.149	5.50
	5	1.17	0.129	0.143	0.198	99.2	0.0447	0.106	0.154	1.40	6.00	31.1	0.156	225	17.4	2.80	3.88	0.348	2.31	3.55	5.33	1.11	0.175	5.21
	6	1.05	0.133	0.0330	0.158	99.4	0.0425	0.0903	0.141	1.26	7.62	44.7	0.143	107	14.2	1.60	3.31	0.380	3.27	4.39	2.96	1.06	0.283	7.05
JLW-60	1	2.33	0.609	5.37	2.81	81.9	0.958	4.34	4.04	2.31	263	1610	1.06	177	62.4	10.6	15.1	4.69	24.8	85.7	36.6	6.95	4.03	10.3
	2	1.05	0.457	1.41	1.04	92.4	0.502	3.20	1.00	1.17	117	4280	0.704	424	26.6	5.97	10.2	2.50	10.8	22.1	12.8	4.20	7.57	13.3
	3	1.13	0.347	1.22	0.861	94.9	0.374	1.44	0.844	1.29	106	2640	0.474	263	22.3	5.22	9.00	1.70	7.38	16.3	12.0	3.95	6.17	10.7
	4	0.863	0.243	0.985	0.714	80.2	0.281	0.553	17.0	0.837	62.3	1360	0.815	265	17.5	5.23	8.26	1.25	4.56	10.7	10.9	3.01	2.22	13.9
	5	0.903	0.281	1.03	0.746	90.8	0.393	0.624	6.12	0.992	62.2	1090	0.419	337	35.0	4.54	6.65	3.61	17.2	41.9	20.6	2.95	1.78	9.99
	6	0.802	0.263	1.67	0.952	92.6	0.524	0.377	3.57	0.899	66.0	708	0.457	341	24.4	5.45	8.02	1.58	6.13	16.3	31.1	3.47	1.56	13.4

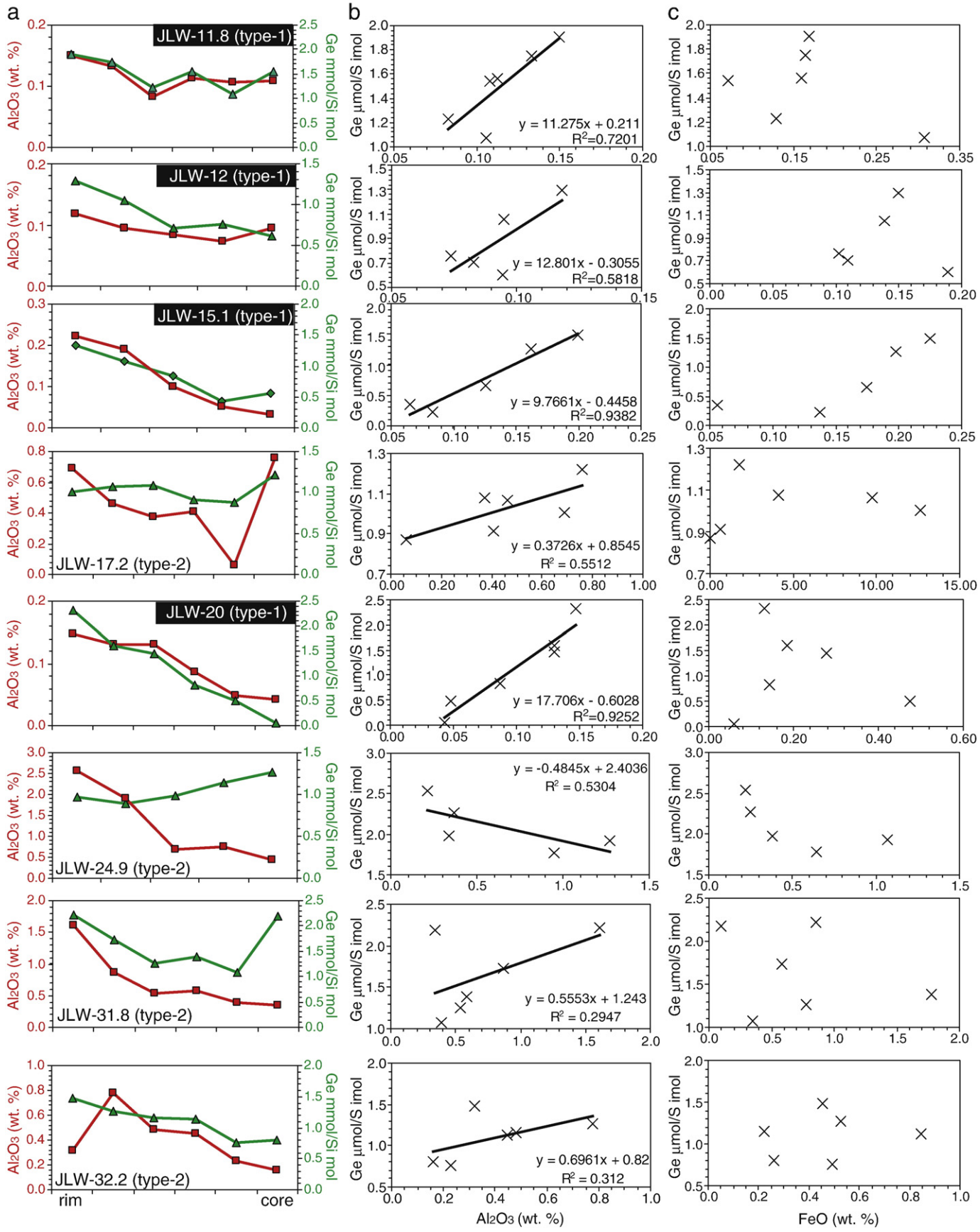

Fig. 4. (a) Variation in Al content (Al_2O_3 wt.%, squares) and Ge/Si ratio (µmol/mol, triangles) from the outer rim to the inner core of chert nodules. (b) Correlation between Al content and Ge/Si ratio of different chert nodules. Best fit lines and correlation coefficients (R-squared values) are shown. (c) Crossplots showing Fe content (FeO wt.%) vs. Ge/Si ratio. The relative uncertainty for Ge/Si is better than 8% (1σ).

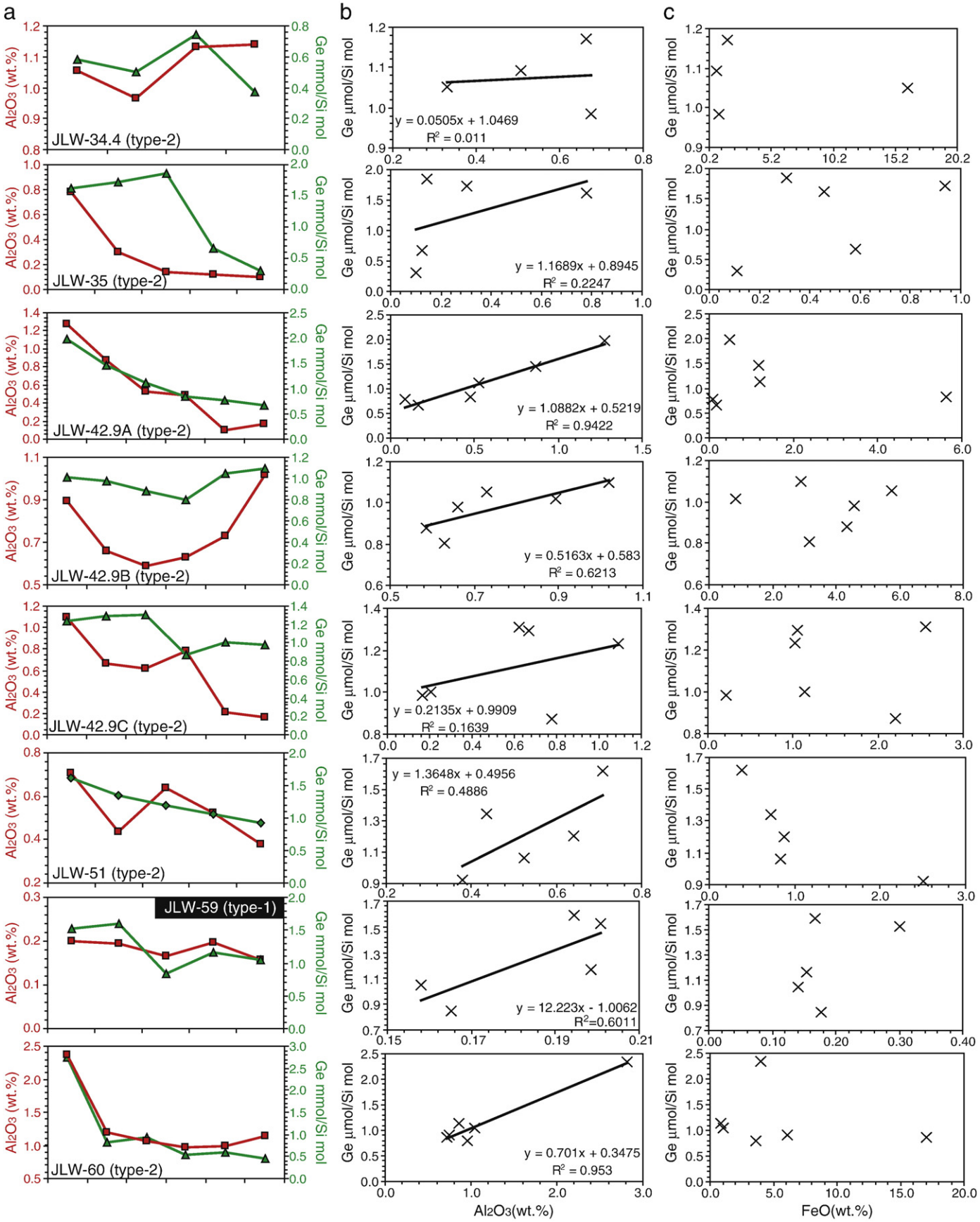

Fig. 4 (*continued*).

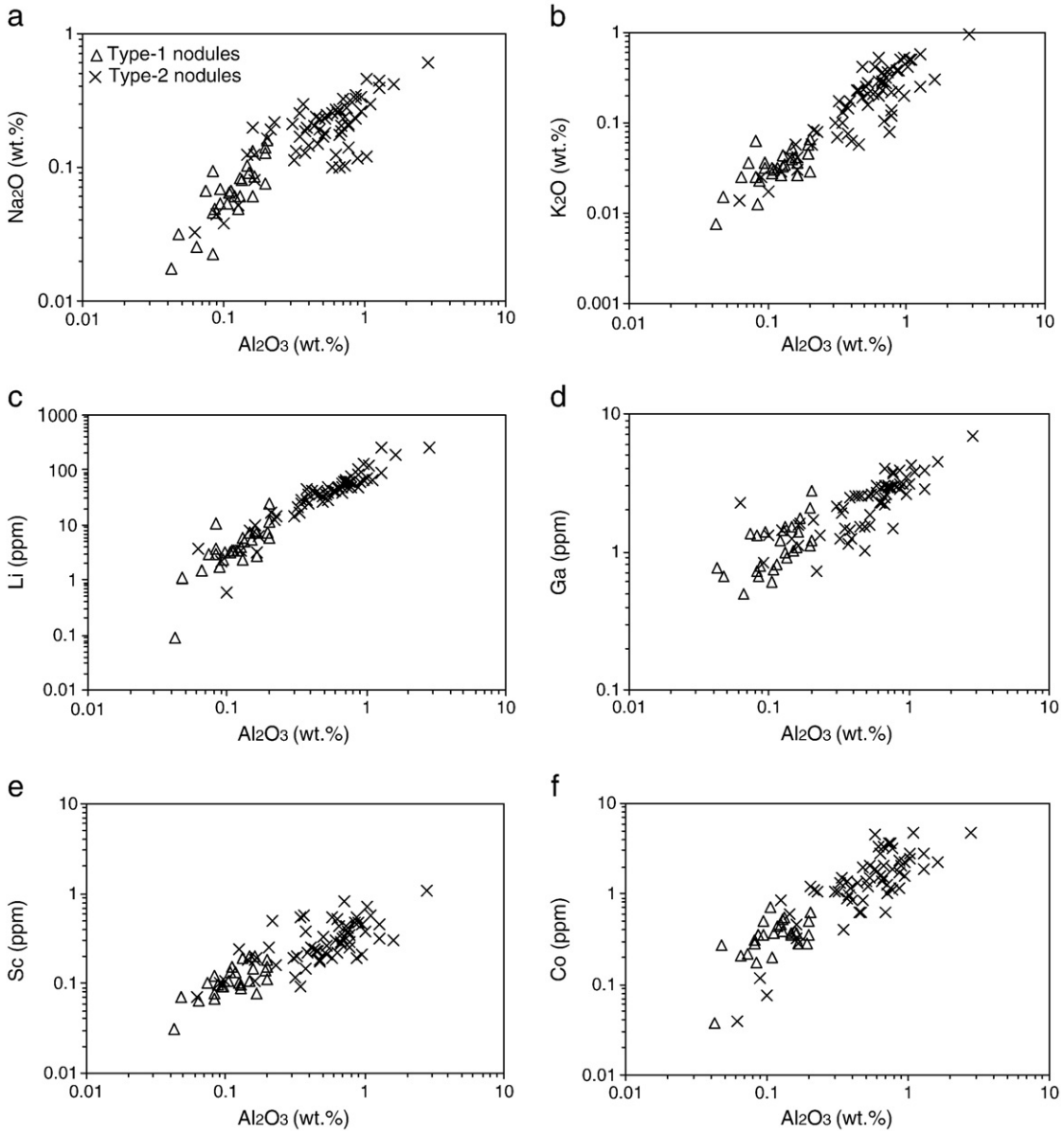

Fig. 5. Crossplots showing correlation of elemental contents. (a) Al vs. Na; (b) Al vs. K; (c) Al vs. Li; (d) Al vs. Ga. (e) Al vs. Sc; (f) Al vs. Co. All plots use log scale on both axes.

derived from the same porewater, $(Ge/Si)_{SiO2}$ of Type-1 chert nodules should also be greater than Type-2 nodules, but this is inconsistent with our observation that Type-1 nodules have lower $(Ge/Si)_{SiO2}$ values (smaller intercepts) than Type-2 nodules (Fig. 4).

Thus, simple mixing between clays and pure silica derived from the same porewaters does not explain the association of the high $(Ge/Si)_{alum}$ and low $(Ge/Si)_{SiO2}$ in Type-1 nodules. The data demand a more complex model, and we propose that redistribution of Ge from a third phase, whose abundance correlates with clays and has an even higher affinity for Ge, could explain the data. Two candidates of this third phase are Fe-Mn oxyhydroxides and organic matter. It is well known that Ge can be enriched in iron oxides such as goethite and hematite (Bernstein, 1985). However, if iron oxides had contributed most of the Ge in the chert nodules, a positive correlation between Ge/Si and Fe would be expected, but this is not the case (Fig. 4c).

The total organic carbon content in the Member II carbonates and mudstones is very high (McFadden et al., 2008), and there are also abundant organic particles in Member II chert nodules (McFadden et al., 2009). As discussed above, disseminated pyrite in Type-2 chert nodules is indicative of bacterial sulfate reduction, which converts porewater sulfate to sulfide via oxidation of organic matter. The fact that the Ge/Si of the inferred Al-rich endmember in Type-2 chert nodules are lower than the pyrite-poor Type-1 chert nodules, suggests that there may be some relationship between organic matter and Ge/Si. Indeed, it has been shown experimentally that Ge–organic complexes can form through chelation of Ge with various organic ligands in a variety of pH conditions. For example, Ge is chelated by catechol (di-phenol) in neutral to basic solutions and by carboxylic acid in acidic solutions (Pokrovski et al., 2000; Pokrovski and Schott, 1998; Viers et al., 1997a). In contrast, negligible (<0.1%) Si–organic complexes are observed in experiments (Pokrovski et al., 2000; Pokrovski and Schott, 1998). For example, river waters in Cameroon contain high concentrations of dissolved organic carbon (20 mg/L), dominated by humic acids with carboxylic and phenolic functional groups (Viers et al., 1997b). In such waters, most Ge is chelated with the humic acids, while Si occurs primarily as inorganic Si $(OH)_4$ species (Viers et al., 1997b). Thus, in the presence of organic

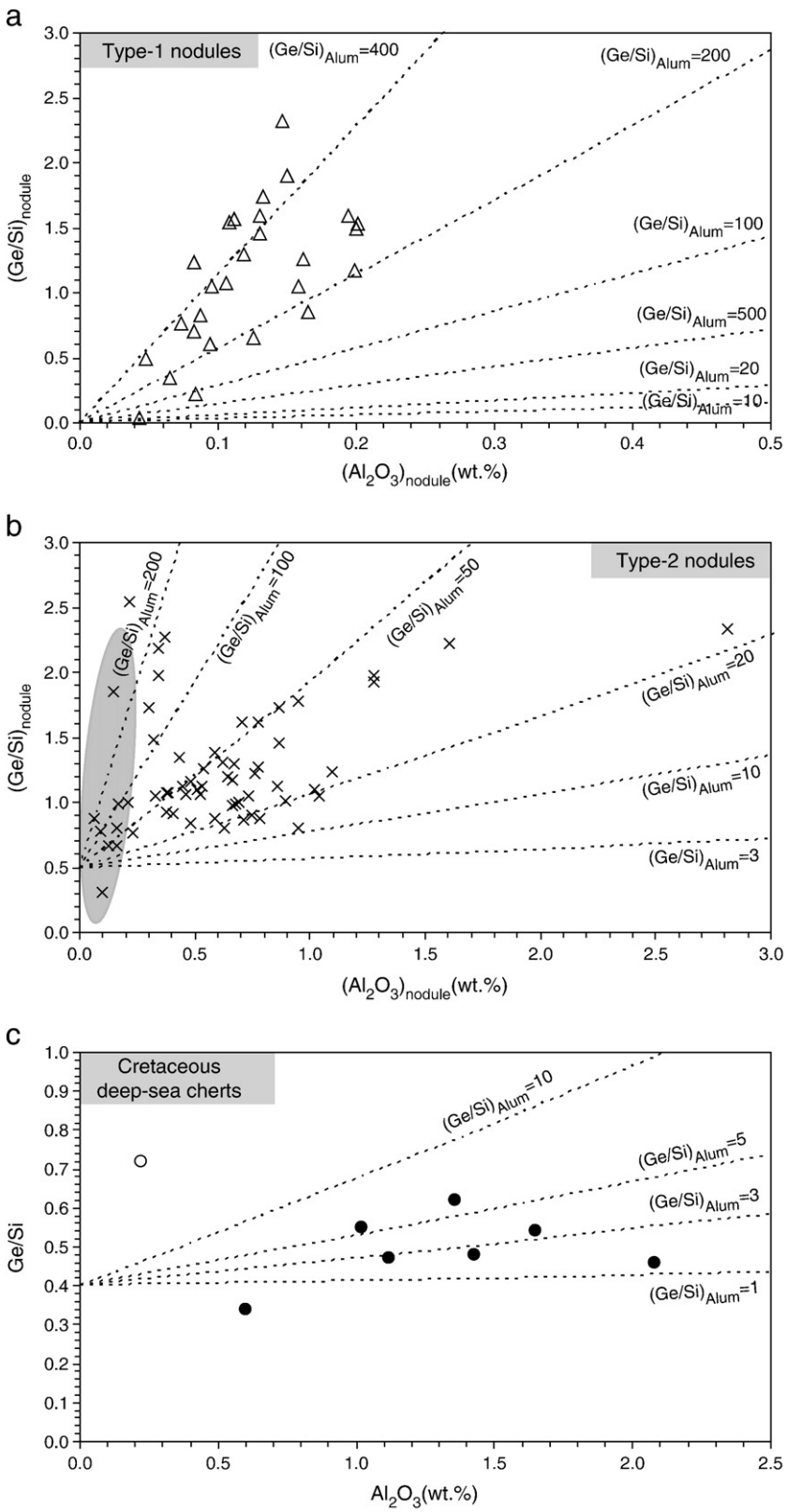

Fig. 6. Crossplots showing the correlation between Al content (Al_2O_3 wt.%) and Ge/Si ratio (μmol/mol) of Doushantuo chert nodules and the Cretaceous deep-sea cherts. The dashed lines are mixing lines between pure chert and clays with different $(Ge/Si)_{alum}$ values, assuming clay mineral is smectite with $Al_2O_3/SiO_2 = 0.25$. (a) Type-1 chert nodules (triangles), assuming $(Ge/Si)_{SiO2} = 0$; (b) Type-2 chert nodules (crosses), assuming $(Ge/Si)_{SiO2} = 0.5$. The shaded area indicates the range of Type 1 chert nodule data. (c) Cretaceous deep-sea cherts, assuming $(Ge/Si)_{SiO2} = 0.4$. The open circle represents sample with hydrothermal quartz (data from Rouxel et al., 2006).

compounds, the geochemical behaviors of Ge and Si can be decoupled, resulting in Ge-rich and Si-poor organic complexes. This property, combined with the well-known propensity for clays to adsorb organic matter (Keil et al., 1994; Mayer et al., 2004), suggests that the enriched Ge in the clay-rich endmember could be explained by co-deposition of clays and organic matter, the latter enriched in Ge–organic complexes.

We now return to the significance of the different Ge/Si vs. Al trends in the two types of chert nodules. The near-zero to slightly negative intercept and steep slope of Ge/Si–Al arrays in Type-1 chert nodules indicate that the pure chert endmember contains negligible Ge ($(Ge/Si)_{SiO2}$ ~ 0) and the Al-rich endmember $(Ge/Si)_{alum}$ is very high, contrasting with Type-2 chert nodules, which have a $(Ge/Si)_{SiO2}$ value of ~0.5 and a lower $(Ge/Si)_{alum}$ value. The simplest interpretation of these differences is that Ge in Type-1 chert nodules is solely associated with the Al-rich endmember, most likely in the form of Ge–organic complexes adsorbed on clays. In Type-2 chert nodules, Ge occurs in both the Al-rich endmember and the pure chert endmember, suggesting that Ge may substitute Si in silica and may also occur as Ge–organic complexes absorbed to clays. As mentioned above, Type-2 chert nodules contain abundant disseminated pyrite in silica core, but Type-1 chert nodules do not. We speculate that bacterial sulfate reduction (Habicht and Canfield, 1997) may have redistributed Ge from clay–organic complexes to pure chert in Type-2 chert nodules. Degradation of organic matter via bacterial sulfate reduction may have resulted in the partial decomposition of Ge–organic complexes, lowering the Ge/Si ratio of the clay–organic complexes and releasing Ge in the form of inorganic $Ge(OH)_4$ species that is subsequently incorporated in the pure silica endmember. The redistribution of Ge can explain the positive intercept and the lower $(Ge/Si)_{alum}$ inferred for Type-2 chert nodules. The poor correlation of Ge/Si vs. Al in Type-2 chert nodules may be attributed to bacterial sulfate reduction. Bacterial sulfate reduction may have been localized and variably modified Ge–organic–clay complex, resulting in heterogeneity in the composition of the Ge–organic–clay complex. Moreover, the subsequent redistribution of Ge that is released from Ge–organic–clay complex by bacterial sulfate reduction into different minerals phases would also generate heterogeneity and result in poor correlations between Ge/Si ratios and Al contents.

6.3. Paleoenvironment implications

The diagenetic origin of the Doushantuo chert nodules implies that the Ge/Si systematics reflects the Doushantuo porewater geochemistry. If our interpretations are correct, most Doushantuo porewater Ge was in the form of Ge–organic–clay complexes, and porewater inorganic $Ge(OH)_4$ may have been derived from the degradation of Ge–organic complexes.

In modern aqueous environments, Ge–organic complexes are present in both terrestrial and marine waters. For example, Ge in the Nsimi-Zoetele watershed in Cameroon is dominated by Ge–humic acid complex (Viers et al., 1997b), because humic substances are the main component of modern terrestrial DOC. Methylgermanium is another type of Ge–organic complex that most likely accumulates in polluted rivers, in which methylgermanium concentrations are 3–100 times higher than in pristine rivers (Lewis et al., 1989). Discharge of polluted river waters makes methylgermanium the only predominant Ge–organic complex in the ocean, accounting for ~80% of Ge in seawater, with the rest represented by inorganic $Ge(OH)_4$ (Bruland and Lohan, 2003; Lewis et al., 1989). Even in reduced sediments where porewater has high concentrations of DOC (up to ~20 mg/L), methylgermanium is still the only Ge–organic complex of significant concentration (McManus et al., 2003). Once in the ocean, methylgermanium is extremely conservative in open oceans although it can be decomposed under anoxic conditions (Lewis et al., 1989). Methylgermanium is believed to be derived from reaction between anthropogenic sewage treatment and coal-ash contaminations (Lewis et al., 1989). As there is no evidence for *de novo* methylgermanium generation in the seawater, we speculate that in the absence of anthropogenic pollution, Ge–organic complex in the Doushantuo basin may have come from a terrestrial source of Ge–humic acid complex.

A terrestrial source of Ge–organic complex would indicate that the depositional and diagenetic environments of the Doushantuo Formation were influenced by terrestrial fluxes, particularly if the Yangtze Gorges area represents a restricted basin during the early Ediacaran Period (Ader et al., 2009). It is hypothesized that the lower Doushantuo Formation in the Yangtze Gorges area was deposited in an alkaline lake that was completely isolated from the world ocean during the early Ediacaran Period (Bristow et al., 2009). A lacustrine environment would be strongly influenced by terrestrial fluxes of Ge–organic complexes, however sedimentological, chemostratigraphic, and paleontological data suggest that the Doushantuo basin was connected with global oceans during the early Ediacaran Period (Jiang et al., 2007; McFadden et al., 2009; Vernhet et al., 2006; Zhu et al., 2007). The balance of data leads us to favor the restricted basin model (Ader et al., 2009) over the isolated lake interpretation (Bristow et al., 2009). Further investigation of the Ge/Si systematics in deep water cherts will provide a test of these hypotheses.

It is also possible that, the inner shelf basin in the Yangtze Gorges area (Jiang et al., 2007; Vernhet et al., 2006; Zhu et al., 2007) may have had different chemistry than Phanerozoic oceans. The absence of Ge–organic complexes (except methylgermanium) in the modern oceans may be attributed to the low DOC concentration (47 μM), because formation of Ge–organic complex requires high DOC concentration up to mM (Pokrovski and Schott, 1998). In contrast, it is hypothesized that DOC concentration in anoxic Neoproterozoic deep oceans could be several orders of magnitudes higher than in modern oceans (Rothman et al., 2003), and several geochemical studies of Ediacaran successions, including the Doushantuo Formation in South China, have provided support for this hypothesis (Fike et al., 2006; Li et al., 2010; McFadden et al., 2008). Thus, it is possible that marine Ge–organic complexes represented a major form of Ge in the Doushantuo Basin, where DOC contents were high.

7. Conclusions

Two types of diagenetic chert nodules from the Ediacaran Doushantuo Formation (Member II) in the Yangtze Gorges area, South China are recognized. Type-1 chert nodules are poor in disseminated pyrite in the silica core and are characterized by low Al contents and steep positive correlations between Ge/Si and Al, whereas Type-2 chert nodules are rich in disseminated pyrite and have higher Al contents, which poorly correlate with Ge/Si. Both types of chert nodules have Ge/Si ratios much greater than Cretaceous deep-sea cherts and modern biogenic opals, possibly reflecting greater Ge/Si ratios in Ediacaran oceans due to the more effective discrimination against Ge by inorganic opal precipitation relative to diatoms. The relationship between Ge/Si ratios and Al contents of the chert nodules is interpreted using a mixing model involving a pure chert endmember and an Al-rich (clay) endmember, the former characterized by low Ge/Si ratios and the latter by high Ge/Si ratios. We show that the inferred Ge/Si ratio of the clay endmember is much higher than modern marine clays. The high Ge content in the Al-rich endmember is best explained by the presence of organic matter co-deposited with clay. Such organic matter may be the main carrier of Ge due to the strong tendency of Ge to chelate with various organic molecules. The Ge/Si systematics of the Doushantuo chert nodules is consistent with a restricted sedimentary environment with a strong terrestrial influence, although an isolated lacustrine sedimentary model is difficult to reconcile with existing sedimentological, geochemical, and paleontological data. Additionally, the dominance of Ge–organic complexes in the Doushantuo Formation may be attributed to high DOC concentrations in Ediacaran seawater and porewater in the Yangtze Gorges area.

Acknowledgements

This study was supported by the Packard Foundation (to Cin-Ty Lee). We thank Kat McFadden and Chuanming Zhou for field assistance and sample collection, and Bob Gaines, Ganqing Jiang, and Chuanming Zhou for useful discussions.

References

Ader, M., et al., 2009. A multilayered water column in the Ediacaran Yangtze platform? Insights from carbonate and organic matter paired $\delta^{13}C$. Earth and Planetary Science Letters 288 (1–2), 213–227.

Awwiller, D.N., 1993. Illite/smectite formation and potassium mass transfer during burial diagenesis of mudrocks; a study from the Texas Gulf Coast Paleocene–Eocene. Journal of Sedimentary Research 63 (3), 501–512.

Bareille, G., Labracherie, M., Mortlock, R.A., Maier-Reimer, E., Froelich, P.N., 1998. A test of $(Ge/Si)_{opal}$ as a paleorecorder of $(Ge/Si)_{seawater}$. Geology 26 (2), 179–182.

Bernstein, L.R., 1985. Germanium geochemistry and mineralogy. Geochimica et Cosmochimica Acta 49 (11), 2409–2422.

Bristow, T.F., et al., 2009. Mineralogical constraints on the paleoenvironments of the Ediacaran Doushantuo Formation. Proceedings of the National Academy of Sciences 106 (32), 13190–13195.

Bruland, K.W., Lohan, M.C., 2003. Controls of trace metals in seawater. In: Holland, H.D., Turekian, K.K. (Eds.), The Oceans and Marine Geochemistry. Treatise on Geochemistry. Elsevier, Oxford, Pergamon, pp. 23–47.

Canfield, D.E., 1998. A new model for Proterozoic ocean chemistry. Nature 396, 450–453.

Canfield, D.E., et al., 2008. Ferruginous conditions dominated later Neoproterozoic deep-water chemistry. Science 321 (5891), 949–952.

Chen, P., 1984. Discovery of Lower Cambrian small shelly fossils from Jijiapo, Yichang, west Hubei and its significance. Professional Papers of Stratigraphy and Palaeontology 13, 49–66.

China Commission on Stratigraphy, 2001. Stratigraphic Guide of China and Its Explanatory Notes (revised edition). Geological Publishing House, Beijing. 42 pp.

Condon, D., et al., 2005. U–Pb ages from the Neoproterozoic Doushantuo Formation, China. Science 308, 95–98.

DeMaster, D.J., 2002. The accumulation and cycling of biogenic silica in the Southern Ocean: revisiting the marine silica budget. Deep Sea Research. Part II: Topical Studies in Oceanography 49 (16), 3155–3167.

Dong, L., et al., 2009. Basal Cambrian microfossils from the Yangtze Gorges area (South China) and the Aksu area (Tarim Block, northwestern China). Journal of Paleontology 83, 30–44.

Elderfield, H., Schultz, A., 1996. Mid-ocean ridge hydrothermal fluxes and the chemical composition of the ocean. Annual Review of Earth and Planetary Sciences 24, 191–224.

Evans, M.J., Derry, L.A., 2002. Quartz control of high germanium/silicon ratios in geothermal waters. Geology 30 (11), 1019–1022.

Fike, D.A., Grotzinger, J.P., Pratt, L.M., Summons, R.E., 2006. Oxidation of the Ediacaran ocean. Nature 444, 744–747.

Froelich, P.N., Andreae, M.O., 1981. The marine geochemistry of germanium: Ekasilicon. Science 213 (4504), 205–207.

Froelich, P.N., Hambrick, G.A., Andreae, M.O., Mortlock, R.A., Edmond, J.M., 1985. The geochemistry of inorganic germanium in natural waters. Journal of Geophysical Research 90 doi:10.1029/JC090iC01p01133.

Froelich, P.N., Mortlock, R.A., Shemesh, A., 1989. Inorganic germanium and silica in the Indian Ocean: biological fractionation during (Ge/Si) opal Formation. Global Biogeochemical Cycles 3 doi:10.1029/GB003i001p00079.

Gehling, J.G., Rigby, J.K., 1996. Long expected sponges from the Neoproterozoic Ediacara fauna of South Australia. Journal of Paleontology 70 (2), 185–195.

Habicht, K.S., Canfield, D.E., 1997. Sulfur isotope fractionation during bacterial sulfate reduction in organic-rich sediments. Geochimica et Cosmochimica Acta 61, 5351–5361.

Hammond, D.E., McManus, J., Berelson, W.M., 2004. Oceanic germanium/silicon ratios: evaluation of the potential overprint of temperature on weathering signals. Paleoceanography 19 doi:10.1029/2003PA000940.

Hammond, D.E., et al., 2000. Diagenetic fractionation of Ge and Si in reducing sediments: the missing Ge sink and a possible mechanism to cause glacial/interglacial variations in oceanic Ge/Si. Geochimica et Cosmochimica Acta 64 (14), 2453–2465.

Hesse, R., 1989. Silica diagenesis: origin of inorganic and replacement cherts. Earth Science Reviews 26, 253–284.

Jiang, G., Kaufman, A.J., Christie-Blick, N., Zhang, S., Wu, H., 2007. Carbon isotope variability across the Ediacaran Yangtze platform in South China: Implications for a large surface-to-deep ocean $\delta^{13}C$ gradient. Earth and Planetary Science Letters 261 (1–2), 303–320.

Jiang, G., Kennedy, M.J., Christie-Blick, N., Wu, H., Zhang, S., 2006. Stratigraphy, sedimentary structures, and textures of the Late Neoproterozoic Doushantuo cap carbonate in South China. Journal of Sedimentary Research 76, 978–995.

Jiang, G., Sohl, L.E., Christie-Blick, N., 2003. Neoproterozoic stratigraphic comparison of the Lesser Himalaya (India) and Yangtze block (south China): Paleogeographic implications. Geology 31, 917–920.

Keil, R.G., Tsamakis, E., Fuh, C.B., Giddings, J.C., Hedges, J.I., 1994. Mineralogical and textural controls on the organic composition of coastal marine sediments: hydrodynamic separation using SPLITT-fractionation. Geochimica et Cosmochimica Acta 58 (2), 879–893.

King, S.L., Froelich, P.N., Jahnke, R.A., 2000. Early diagenesis of germanium in sediments of the Antarctic South Atlantic: in search of the missing Ge sink. Geochimica et Cosmochimica Acta 64 (8), 1375–1390.

Kurtz, A.C., Derry, L.A., Chadwick, O.A., 2002. Germanium-silicon fractionation in the weathering environment. Geochimica et Cosmochimica Acta 66, 1525–1537.

Lee, C.-T.A., Oka, M., Luffi, P., Agranier, A., 2008. Internal distribution of Li and B in serpentinites from the Feather River Ophiolite, California based on laser ablation inductively coupled plasma mass spectrometry. Geochemistry, Geophysics, Geosystems 9 doi:10.1029/2008GC002078.

Lewis, B.L., Andreae, M.O., Froelich, P.N., 1989. Sources and sinks of methylgermanium in natural waters. Marine Chemistry 27 (3–4), 179–200.

Li, C.-W., Chen, J.-Y., Hua, T.-E., 1998. Precambrian sponges with cellular structures. Science 279, 879–882.

Li, C., et al., 2010. A stratified redox model for the Ediacaran ocean. Science 328 (5974), 80–83.

Li, Z.-X., et al., 2007. Early history of the eastern Sibao Orogen (South China) during the assembly of Rodinia: new mica $^{40}Ar/^{39}Ar$ dating and SHRIMP U–Pb detrital zircon provenance constraints. Precambrian Research 159, 79–94.

Lugolobi, F., Kurtz, A.C., Derry, L.A., 2010. Germanium-silicon fractionation in a tropical, granitic weathering environment. Geochimica et Cosmochimica Acta 74 (4), 1294–1308.

Maliva, R.G., Siever, R., 1989. Nodular chert formation in carbonate rocks. Journal of Geology 97 (4), 421–433.

Mayer, L.M., Schick, L.L., Hardy, K.R., Wagai, R., McCarthy, J., 2004. Organic matter in small mesopores in sediments and soils. Geochimica et Cosmochimica Acta 68 (19), 3863–3872.

McFadden, K.A., et al., 2008. Pulsed oxidation and biological evolution in the Ediacaran Doushantuo Formation. Proceedings of the National Academy of Sciences 105, 3197–3202.

McFadden, K.A., Xiao, S., Zhou, C., Kowalewski, M., 2009. Quantitative evaluation of the biostratigraphic distribution of acanthomorphic acritarchs in the Ediacaran Doushantuo Formation in the Yangtze Gorges area, South China. Precambrian Research 173 (1–4), 170–190.

McManus, J., Hammond, D.E., Cummins, K., Klinkhammer, G.P., Berelson, W.M., 2003. Diagenetic Ge–Si fractionation in continental margin environments: further evidence for a nonopal Ge sink. Geochimica et Cosmochimica Acta 67 (23), 4545–4557.

Mortlock, R.A., Froelich, P.N., 1987. Continental weathering of germanium: in the global river discharge. Geochimica et Cosmochimica Acta 51 (8), 2075–2082.

Mortlock, R.A., et al., 1993. Silica and germanium in Pacific Ocean hydrothermal vents and plumes. Earth and Planetary Science Letters 119 (3), 365–378.

Pokrovski, G.S., Martin, F., Hazemann, J.-L., Jacques, S., 2000. An X-ray absorption fine structure spectroscopy study of germanium–organic ligand complexes in aqueous solution. Chemical Geology 163 (1–4), 151–165.

Pokrovski, G.S., Schott, J., 1998. Experimental study of the complexation of silicon and germanium with aqueous organic species: implications for germanium and silicon transport and Ge/Si ratio in natural waters. Geochimica et Cosmochimica Acta 62 (21–22), 3413–3428.

Qian, Y., 1999. Taxonomy and Biostratigraphy of Small Shelly Fossils in China. Science Press, Beijing. 247 pp.

Rothman, D.H., Hayes, J.M., Summons, R.E., 2003. Dynamics of the Neoproterozoic carbon cycle. Proceedings of the National Academy of Sciences of the United States of America 100, 8124–8129.

Rouxel, O., Galy, A., Elderfield, H., 2006. Germanium isotopic variations in igneous rocks and marine sediments. Geochimica et Cosmochimica Acta 70 (13), 3387–3400.

Siever, R., 1992. The silica cycle in the Precambrian. Geochimica et Cosmochimica Acta 56 (8), 3265–3272.

Steiner, M., Mehl, D., Reitner, J., Erdtmann, B.-D., 1993. Oldest entirely preserved sponges and other fossils from the lowermost Cambrian and a new facies reconstruction of the Yangtze Platform (China). Berliner Geowissenschaftliche Abhandlungen (E) 9, 293–329.

Tréguer, P., et al., 1995. The silica balance in the world ocean: a reestimate. Science 268 (5209), 375–379.

Vernhet, E., Heubeck, C., Zhu, M.Y., Zhang, J.M., 2006. Large-scale slope instability at the southern margin of the Ediacaran Yangtze platform (Hunan province, central China). Precambrian Research 148 (1–2), 32–44.

Vernhet, E., Reijmer, J.J.G., 2010. Sedimentary evolution of the Ediacaran Yangtze platform shelf (Hubei and Hunan provinces, Central China). Sediment. Geol. 225, 99–115.

Viers, J., et al., 1997a. Chemical weathering in the drainage basin of a tropical watershed (Nsimi-Zoetele site, Cameroon): comparison between organic-poor and organic-rich waters. Chemical Geology 140 (3–4), 181–206.

Viers, J., et al., 1997b. Chemical weathering in the drainage basin of a tropical watershed (Nsimi-Zoetele site, Cameroon): comparison between organic-poor and organic-rich waters. Chemical Geology 140 (3–4), 181–206.

Wang, J., Li, Z.-X., 2003. History of Neoproterozoic rift basins in South China: implications for Rodinia break-up. Precambrian Research 122 (1–4), 141–158.

Wheat, C.G., McManus, J., 2008. Germanium in mid-ocean ridge flank hydrothermal fluids. Geochemistry, Geophysics, Geosystems 9 doi:10.1029/2007GC001892.

Xiao, S., Schiffbauer, J.D., McFadden, K.A., Hunter, J., 2010. Petrographic and SIMS pyrite sulfur isotope analyses of Ediacaran chert nodules: implications for microbial processes in pyrite rim formation, silicification, and exceptional fossil preservation. Earth and Planetary Science Letters 297 (3–4), 481–495.

Xiao, S., Zhang, Y., Knoll, A.H., 1998. Three-dimensional preservation of algae and animal embryos in a Neoproterozoic phosphorite. Nature 391, 553–558.

Zhao, Z., et al., 1988. The Sinian System of Hubei. China University of Geosciences Press, Wuhan. 205 pp.

Zhou, C., Xiao, S., 2007. Ediacaran $\delta^{13}C$ chemostratigraphy of South China. Chemical Geology 237, 107–126.

Zhou, C., Xie, G., McFadden, K., Xiao, S., Yuan, X., 2007. The diversification and extinction of Doushantuo-Pertatataka acritarchs in South China: causes and biostratigraphic significance. Geological Journal 42, 229–262.

Zhu, M., Gehling, J.G., Xiao, S., Zhao, Y.-L., Droser, M., 2008. A new eight-armed Ediacara fossil preserved in contrast taphonomic windows from China and Australia. Geology 36, 867–870.

Zhu, M., Zhang, J., Yang, A., 2007. Integrated Ediacaran (Sinian) chronostratigraphy of South China. Palaeogeography, Palaeoclimatology, Palaeoecology 254 (1–2), 7–61.